Mechanical strength and electrical conductivity of Ni-YSZ cermets fabricated by viscous processing

LAILA GRAHL-MADSEN
IRD Fuel Cells A/S, Kullinggade 31, DK-5700, Svendborg, Denmark

PETER HALVOR LARSEN, NIKOLAOS BONANOS
Materials Research Department, Risø National Laboratory, DK-4000 Roskilde, Denmark

JOHN ENGELL
PF&U Mineral Development ApS, Kullinggade 31, DK-5700 Svendborg, Denmark

SØREN LINDEROTH
Materials Research Department, Risø National Laboratory, DK-4000 Roskilde, Denmark

Published online: 4 February 2006

A method for manufacturing of profiled Ni-YSZ anode support sheets by water-based viscous processing has been developed. Mechanical and electrical properties have been studied and were found to correlate with the microstructures and heat treatment. Electrical conductivities in the order of 1000 S/cm were obtained at 1000°C. The results reveal a linear dependence between the conductivity and pre-test reduction temperature: the conductivity increases by a factor of about 6 when reducing the anode support at 1000°C compared to 650°C. Heat treatment after the reduction at low temperature does not improve the conductivity. Insignificant degradation with time was observed at test temperatures between 800 and 1000°C. However, very high electrical loads did lower the conductivity. The developed microstructure withstood two redox cycles without decrease in conductivity. The mechanical strength of components, optimised with respect to both conductivity and strength, showed little change in strength upon reduction, i.e. when changing the structure from NiO/YSZ to Ni/YSZ, revealing that the YSZ matrix governs the mechanical strength.

1. Introduction

Ni-YSZ anode supported thin electrolyte cells represent the state-of-the-art in planar solid oxide fuel cells [1]. An additional Ni-YSZ component (anode support) serves in the present design as the mechanical backbone, as current collector and as fuel distributor [2, 3]. The YSZ matrix provides the mechanical strength and percolating Ni particles the electronic conductivity. The large amount of Ni needed (about 40 vol%) in order to obtain percolation [4] may cause redox stability problems due to large volume changes during redox cycling. The present paper comprises one simple fabrication route and the resulting characteristics of such an additional anode support stack component.

The manufacturing of anode supports is carried out by the use of several techniques, such as tape casting [2] or calendering [5]. In this paper we present a study on Ni-YSZ components fabricated by viscous processing: calendering followed by shaping of gas distribution channels. The result of the processing is critically dependent on the characteristics of the ceramic powder(s) used, the binder-system chosen, the solids loading in the resulting plastic masses, and the parameter settings used during mixing and forming.

The work done at Argonne National Laboratory [6, 7] and Allied Signal Aerospace Corporation [5, 8] is based on the use of a binder-system composed of a thermoplastic polymer and a plasticizer. The ingredients are mixed together in a high-speed mixer, where the heat generated by friction softens the binder, and allows the formation of a homogeneous plastic mass [9]. Alternatively, the binder-system may be softened or dissolved in a suitable solvent (EtOH/MEK for the PVB/DBP system; H_2O for the system used by Kendall *et al.* [10] and for the one used by Shoho and Morinaga [11]). In the present study a different very environmentally friendly H_2O based binder system has been chosen. Seven different NiO/8YSZ viscous masses have been prepared.

0022-2461
DOI: 10.1007/s10853-005-3647-3

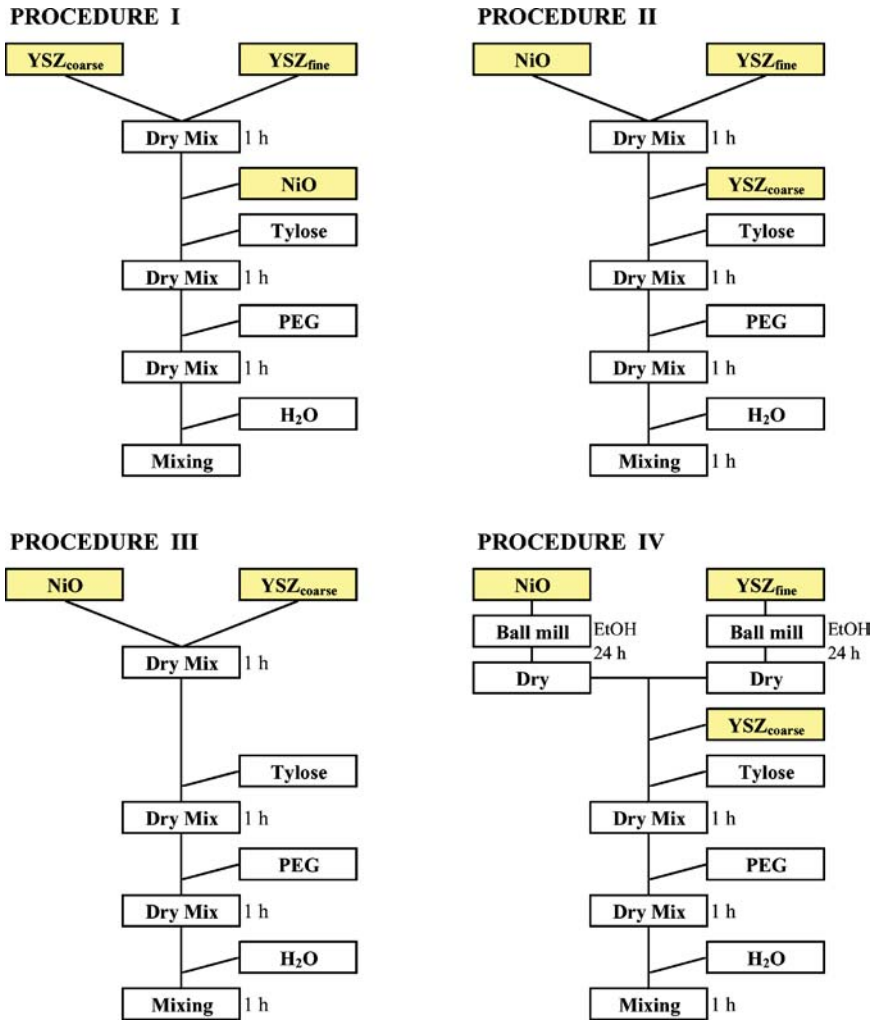

Figure 1 Procedures used for mixing of the NiO/YSZ masses.

Mechanical tests were performed before and after reduction. The effects of the reduction conditions were examined and the reduction temperature is found to be an important parameter for the initial conductivity. Redox stability of the conductivity is reported.

2. Experimental

2.1. Chemicals and viscous processing

The powders used are NiO (Merck) and 8 mol% Yttria-stabilized Zirconia (TZ-8Y, TOSOH or MELcoarseSCY1291085, Magnesium Elektron). The water-based binder system employed was composed of methyl-hydroxy-ethyl-cellulose (Tylose MH 300P, Hoechst, or Tylose MH 300P2, Clariant) and polyethylene glycol 400 (PEG, for synthesis, Merck-Schuchardt). The NiO has been used either as received or as calcined (1300°C, 2 h with subsequent ball milling).

The mean particle size ($d_{50\%}$, SediGraph 5000 ET) of the as-received black NiO was 7.6 μm, while it was 5.4 μm for the calcined and ball milled NiO. The as received Tosoh zirconia powder had the following characteristics: specific surface area 13.3 m^2/g, $d_{50\%} = 0.14$ μm, and a crystallite size 24 nm. Coarse-grained near spherical 8YSZ particles were prepared by calcination of the as-received Tosoh powder at 1400°C for 20 h. The powders prepared in this way were sieved at 90 μm (98 wt% $\leq$90 μm) before use. The sieved powder has an average grain size of 34 μm as determined by optical microscopy. The MELcoarseSCY1291085 powder having a $d_{50\%}$ of 16 μm was used as received. The procedures used for mixing of the masses are shown in Fig. 1 (Procedure I: NYZ-1 & NYZ-4 to NYZ-6; Procedure II: NYZ-2; Procedure III: NYZ-3; and Procedure IV: NYZ-7). The dry mixing was done by ball milling. The desired amount of water was added during either mixing in a Z-mixer for one hour or by hand mixing.

The compositions of the plastic masses prepared are given in Table I. Upon firing, the composition of the masses is close to 44 wt% YSZ and 56 wt% NiO (40 vol% Ni upon reduction). The ratio between coarse- and fine-grained YSZ is 4 as suggested by Itoh *et al.* [12] except for composition NYZ-3, which contains no fine-grained YSZ.

The viscous masses prepared were shaped into $\approx$1 mm thick sheets using a roller machine. During rolling the masses were wrapped in plastic film in order to minimize

TABLE I Compositions of viscous masses and density of green and sintered materials

		Composition							Density	
		NiO		8YSZ						
Mass	Mixing (Fig. 1)	Raw (wt%)	Calc. (wt%)	Fine (wt%)	Coarse (wt%)	PEG (wt%)	Tylose (wt%)	H_2O (wt%)	Green (%)	Sintered 1500°C (%)
NYZ-1	I	–	42.8	6.7	26.9[a]	4.7	5.1	13.7	47	62
NYZ-2	II	–	42.6	6.7	26.8[b]	4.7	5.1	14.1	47	58
NYZ-3	III	–	42.8		33.6[b]	4.7	5.1	13.7	47	54
NYZ-4	I	–	42.7	6.7	26.8[b]	4.7	5.1	14.0	47	60
NYZ-5	I	–	42.8	6.7	26.9[c]	4.7	5.1	13.7	47	64
NYZ-6	I	40.3	–	6.3	25.3[c]	4.4	4.8	18.9	40	64
NYZ-7	IV	43.5	–	6.9	27.6[b]	4.6	4.5	12.9	47	66

[a]Tosoh TZ-8Y, calcined at 1400°C, $d_{50\%}$=28 μm and d_{max}=45 μm.
[b]Tosoh TZ-8Y, calcined at 1400°C, $d_{50\%}$=34 μm and d_{max}=90 μm.
[c]MELcoarseSCY12 91085, $d_{50\%}$=21 μm, d_{max}=80 μm and $d_{min}\approx$3 μm.

evaporation of water. The sealed masses were rolled in a polyethylene bag to avoid curling during rolling of thin sheets. Upon rolling the sheets were cut into the desired dimensions and dried by one of the following procedures:

1. The cut sheets were placed between alumina or glass plates, and dried at 60°C 75% RH for >1 day. The final drying was done at 110°C until the weight was constant (0.4–1.5 wt% rest H_2O).
2. The cut sheets were first dried in a microwave oven (≈8.8 wt% of water was removed). The supports were then placed between glass plates and dried at 110°C for 17–24 h (≈1.5 wt% residual water).

Using either of the drying schemes described above, the flatness of the resulting sheets depended on the flatness of the plates between which the Ni/YSZ supports were dried (±25 μm).

Anode supports with channels on one side have been prepared by uniaxial pressing of green rolled Ni/YSZ sheets using a pressing tool made of POM plastic (Poly-Oxy-Methylene).

2.2. Characterisation

2.2.1. Sintering

The dry Ni/YSZ supports were sintered at 1500°C on coarse-grained YSZ powder (fraction ≥90 μm) to avoid sticking to the substrate during sintering. The density of sintered samples has been determined by Archimedes' method in water. Linear sintering shrinkage was measured both with a calliper before and after sintering and on dry anode support samples, ≈15 × 5 × 5 mm^3, using a Netzch dilatometer.

2.2.2. Thermal expansion and dimensional change on reduction

Dimensional change upon reduction (1) and thermal expansion coefficient (TEC) of reduced supports (2) were measured using a Setaram 2050 dilatometer with a 75–100 g/cm^2 load on the samples that were presintered at 1500°C in air. The experimental procedure is outlined below:

1. Heat treatment in air to 1100°C with a heating rate of 2°C/min, then cooled to 850°C at which temperature the atmosphere was changed to dry 9%H_2:91%N_2, and finally cooling to room temperature after dimensional equilibrium was reached.
2. TECs were measured during re-heating of the samples to 1100°C with 2°C/min in a dry 9%H_2:91%N_2 atmosphere.

2.2.3. 4-Point bending strength

The four point bending strength was measured at room temperature (RT) on bars sintered at 1500°C for 2 h and on bars sintered and then reduced at 850°C for ≈50 h. The bars were cut before sintering and reduction and surface flaws were not removed prior to the bending tests.

The 4-point bending strength was measured using outer/inner spans 10 mm/5 mm, and a cross head speed of 0.22 mm/min. The median bending strength and Weibull modulus was calculated as originally suggested by Weibull [13] and later advocated by Sullivan and Lauzon [14]. Considering the limited numbers of specimens tested, the statistical calculations should only serve as a rough estimate of the variation among samples.

2.2.4. In-plane conductivity

The in-plane conductivity of anode supports has been measured using the four-point DC measurement technique. Test bars (≈50 ∗ 1 ∗ 7 mm^3) were cut from green dry plates and sintered at 1500°C for 2 h in air. Samples tested at 800–1000°C had four Pt-wires attached using Pt-paste, baked at 1040°C for 2 h in air prior to testing. The test bars were mounted in a closed Kanthal vessel placed in a furnace. The furnace was heated to the test

temperature in ≈5 h and the sample chamber was flushed with N_2 prior to switching to the test gas (9 or 10% H_2 in N_2). The reduction of NiO to Ni was performed at the test temperature, except for two samples (NYZ-2 & NYZ-4), which were reduced during heating (≥600°C). The test gas flow was kept constant (≈100 l/h) in order to maintain a low oxygen partial pressure (p_{O_2}) during testing (10^{-18}–10^{-17} Pa) and to keep the samples reduced during cooling to room temperature. Current was imposed via the outer probes and voltage was measured at the inner probes. The samples were continuously exposed to a constant voltage of 3 V during testing, resulting in a current density of the order of 7 A/cm^2. Typical SOFC current densities are around 1 A/cm^2. Data were collected at two-minute intervals using commercial software (GENIE, Advantech) and an ADAM5000 unit for data transmission (Advantech).

The in-plane conductivity at RT was also measured using the four-point measurement technique. The pre-sintered (1500°C/2 h) NYZ-7 samples were reduced in one of the following two ways:

1. At T_{max} (600–1000°C) in a 9%H_2:91%N_2 atmosphere, or
2. Gradually during heating: RT-600°C: in air, 600°C-T_{max} with 1°C/min in a 1%H_2:99%N_2 atmosphere ($p_{O_2} \leq 10^{-10}$ Pa) switching to 9%H_2:91%N_2 at T_{max}, and leaving the sample under these conditions for 24 hrs.

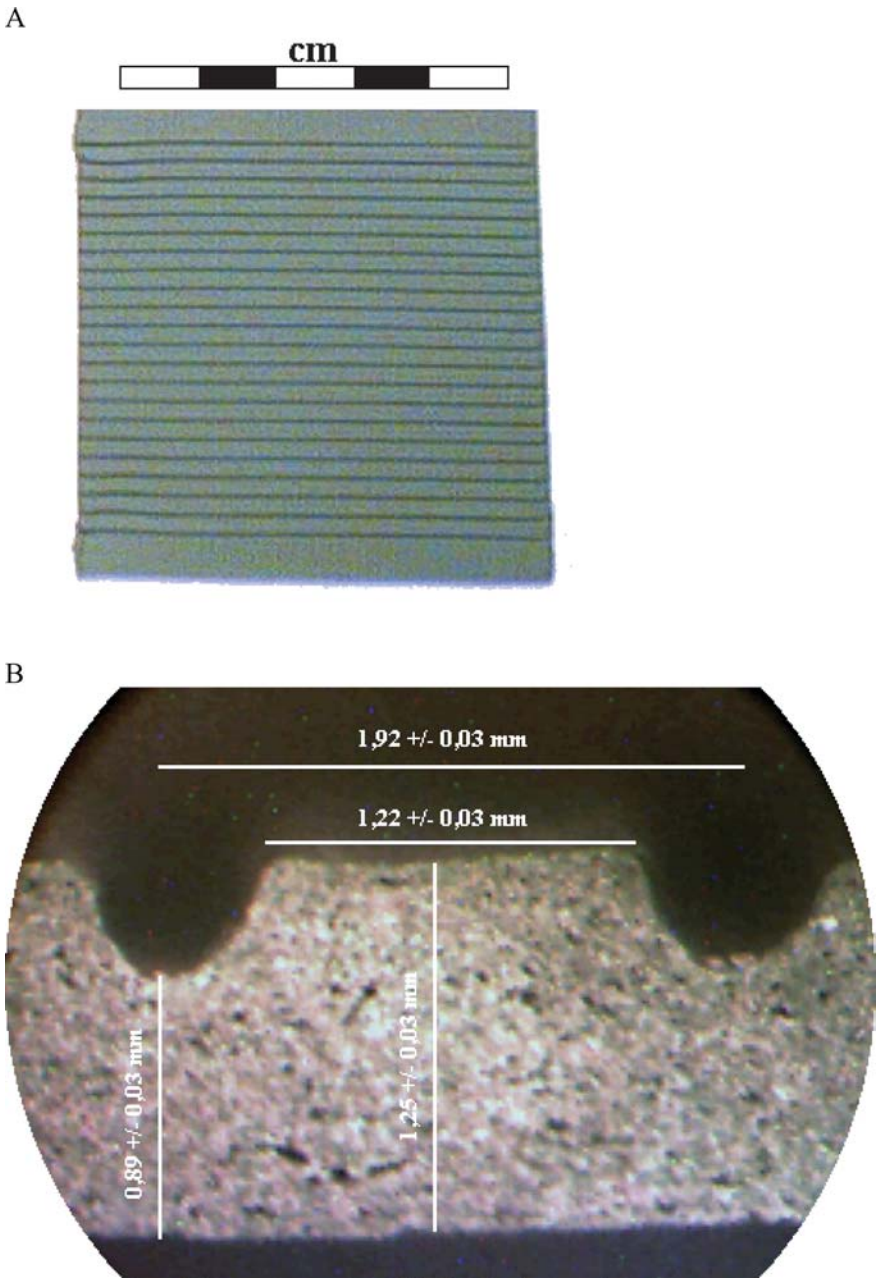

Figure 2 (A) Green anode supports with fuel channels on one side, (B) Cross-section of sintered NYZ-5 with channels.

The reduction conditions outlined in (2) simulate real operating conditions, where the anode is reduced gradually during the first start up.

3. Results and discussion

3.1. Shaping and sintering

The calendering technique offers a fast and simple possibility of imposing fuel channels on either side of the wet calendered sheet. Anode supports with 22 channels on one side are shown in Fig. 2A together with a micrograph of the channels in cross section (Fig. 2B).

The green supports are easy to handle upon drying (110°C). They posses a green density in excess of 40% as shown in Table I together with sintered density. This low density is caused by use of black, un-milled NiO powder having the original dendrite morphology and resulting in a low packing density.

The sintering profiles seen in Fig. 3 divide the samples in two groups:

1. NYZ-1, NYZ-2 & NYZ-4 show some shrinkage (1.5–3.0%) during binder burnout below 400°C, almost no shrinkage between 400 to 1100°C, and minor shrinkage above 1100°C due to sintering.
2. NYZ-6 & NYZ-7 show a relatively small shrinkage during binder burnout at temperatures below 400°C, limited shrinkage in the temperature interval 400–900°C, and a significant increase in the shrinkage rate above 900°C.

The total shrinkage of group 2 samples is significantly higher than that of group 1 samples. The absence of shrinkage during binder burnout for the group 2 samples is probably the result of a high degree of particle-particle contact in the green body(agglomeration). The major difference between the two groups is that the NiO powder used for the second group was as-received, whereas for the remaining compositions it was calcined at 1300°C. From Fig. 3 it is also seen that the use of black as-received NiO powder significantly lowers the onset temperature

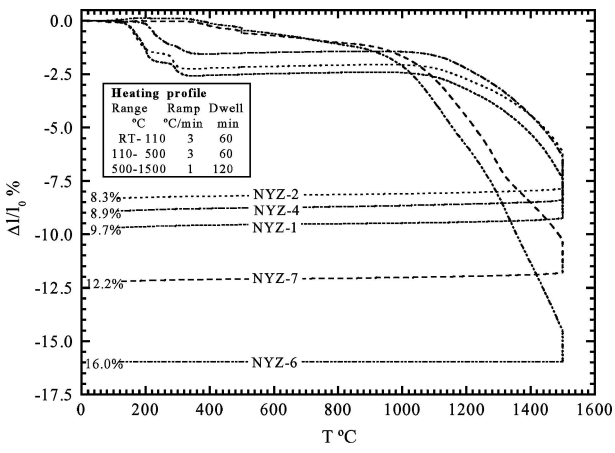

Figure 3 Linear sintering shrinkage measured by dilatometry.

for sintering. The microstructure of group 2 samples with fine <1 micron NiO particles and coarse YSZ particles is illustrated in Fig. 4A by NYZ-7. Despite the poorer packing density of NYZ-7, the final density is almost identical to that of NYZ-6 (cf. Table I).

The difference in bulk densities between plates made of mass NYZ-2 and NYZ-4 having identical composition is most likely due to the different mixing procedures. For NYZ-2, fine-grained 8YSZ was mixed with the NiO in the first step (Procedure II, Fig. 1), while for NYZ-4 the two fractions of 8YSZ powder were mixed before addition of the NiO (Procedure I, Fig. 1). This results in a different spatial distribution of the fine-grained 8YSZ powder, which again affects the sinterability of the green bodies (the microstructures can be compared in Fig. 4B and D, respectively).

Mass NYZ-5 was prepared as NYZ-4 (Procedure I, Fig. 1), except that the coarse YSZ powder used is finer (Table I) and has a sub-angular morphology. This change enhances the sinterability and results in an increased density. NYZ-3 represents a sample fabricated with no fine grained 8YSZ at all and this results not surprisingly in a significantly lower sintered density; the comparatively coarse microstructure is shown in Fig. 4C.

The microstructures obtained upon reduction at 1000°C of some of the differently prepared Ni/YSZ supports are shown in Fig. 5. Comparing Fig. 5A and C shows the effect of fine *versus* coarse NiO powder on the microstructure. In both cases, an excellent percolation of the Ni structure is evident. Samples NYZ-2 and NYZ-4 that are compositionally identical (different mixing procedure) reveals similar Ni microstructures that appear more scattered and less rigid in comparison with the microstructures shown in Fig. 5A and C.

3.2. Thermal expansion and dimensional change during reduction

The thermal expansions were found to be almost independent of the composition as well as the preparation procedure. TEC in the temperature range from RT to 850°C in air and under reducing conditions were 11.8 and 12.4 $\times$ 10^{-6} K^{-1}, respectively (expansion curves not shown here).

The linear contraction during reduction is shown in Fig. 6. The supports based on calcined NiO (NYZ-1, NYZ-2 and NYZ-4) reveal a slower reduction profile in comparison with the supports fabricated with as-received NiO (NYZ-6 & NYZ-7, Table I). In the latter cases, the dimensional change upon reduction is completed after less than 3 h. The reported difference in reduction rate is in correspondence with the NiO grain sizes and microstructures as illustrated in Figs 4 and 5. The finer the NiO grain size, the faster the rate of reduction. The support prepared without fine grained YSZ (NYZ-3) displays the highest shrinkage upon reduction, illustrating that the YSZ does not form a stable network during sintering (cf. Figs 4C and 5C).

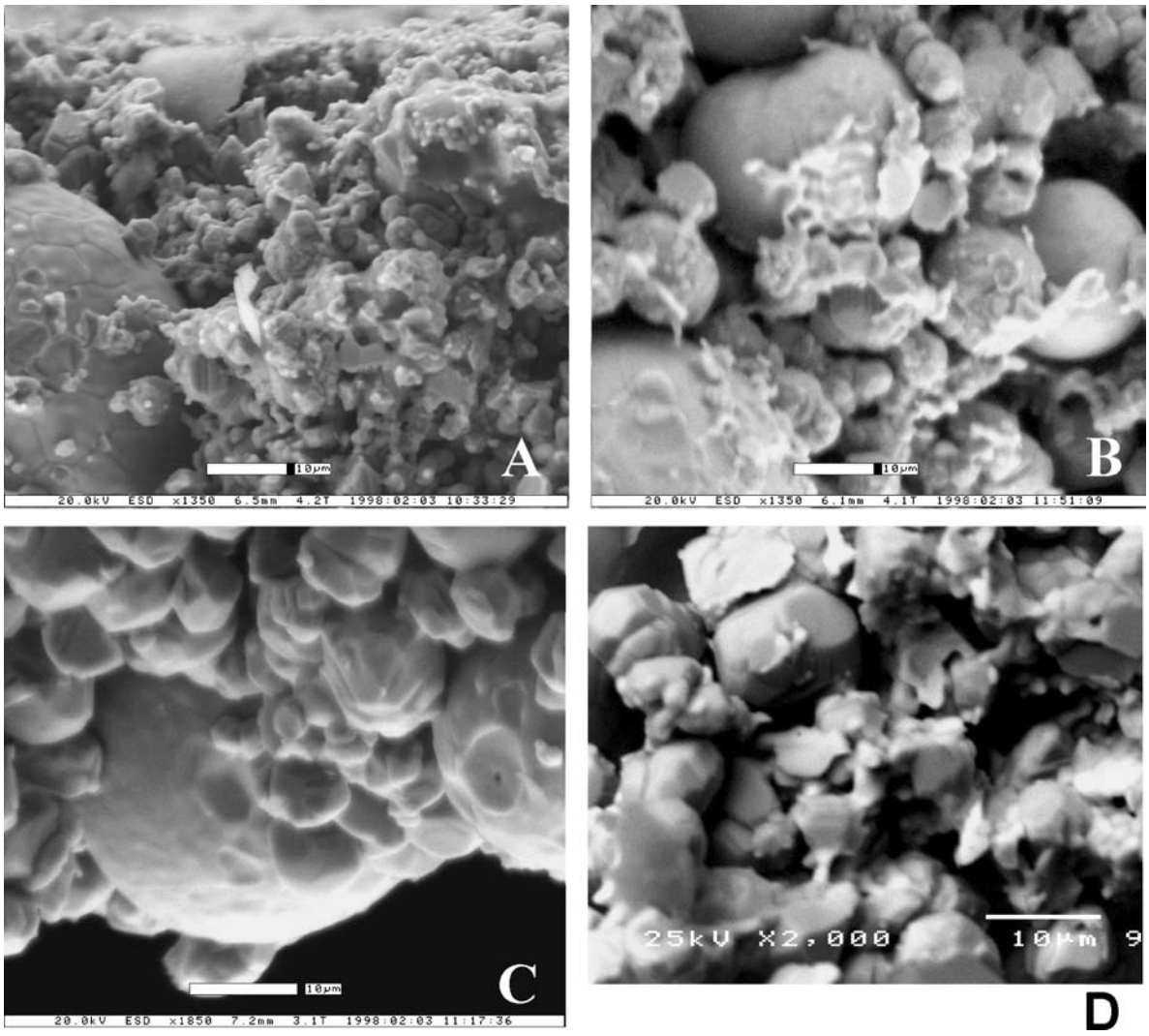

Figure 4 SEM micrographs showing fractured surfaces of the porous Ni/YSZ supports after sintering in air at 1500°C for 2 h. The white scale-bar is 10 μm on all four pictures. A: NYZ-7, B: NYZ-2, C: NYZ-3 and D: NYZ-1. Large spherical particles are YSZ; matrix is a mixture of NiO and fine YSZ.

In summary, the degree of shrinkage is directly related to the strength of the YSZ backbone and this is mainly controlled by the sinterability of the green YSZ structure, but the initial grain size of NiO also plays a minor role as the samples prepared with the most sinter active NiO show the largest shrinkage e.g. NYZ-2 and NYZ-7 is prepared with identical YSZ amount & types, but while NYZ-7 was prepared with black as -receive NiO, was NYZ-2 prepared with calcined NiO.

3.3. Bending strength

The 4-point bending strength of the as-sintered samples divides the supports into three groups. Samples prepared without fine-grained YSZ represent the weakest group. These supports (NYZ-3) were too weak to be tested (the bending strength was estimated to be below 5 MPa), in both the as-sintered and the as-reduced state. The strength of the other two groups is illustrated in Fig. 7. The strength of the ceramic in the strongest group (NYZ-5 and NYZ-7) has a mean value ≈20 MPa, which is twice that of the weaker group. The calculated Weibull modulus ($m \approx 10$) is within the typical range of technical ceramics [15]. There is a strong correlation between the densities and strengths. The three groups have mean densities of 54, 60, and 65, respectively, the strongest group having the highest density.

The strength of the supports depends on the strength of the YSZ structure, as discussed previously, while the texture of the NiO network has a controlling influence on the Ni network formed upon reduction, and thus, on the electronic conductivity and its long-term stability. The weakest group, prepared without fine-grained YSZ powder, shows a coarse-grained NiO network and no or very limited necking between the large spherical zirconia grains (Fig. 4C). The two supports in the strongest group belong to the densest supports fabricated (>64% TD, Table I), which allow a better zirconia network simply by closer physical contact during sintering. However, the density has no apparent influence on the strength of supports with <64% TD because of their high porosity. The two densest and strongest supports are based on different precursor

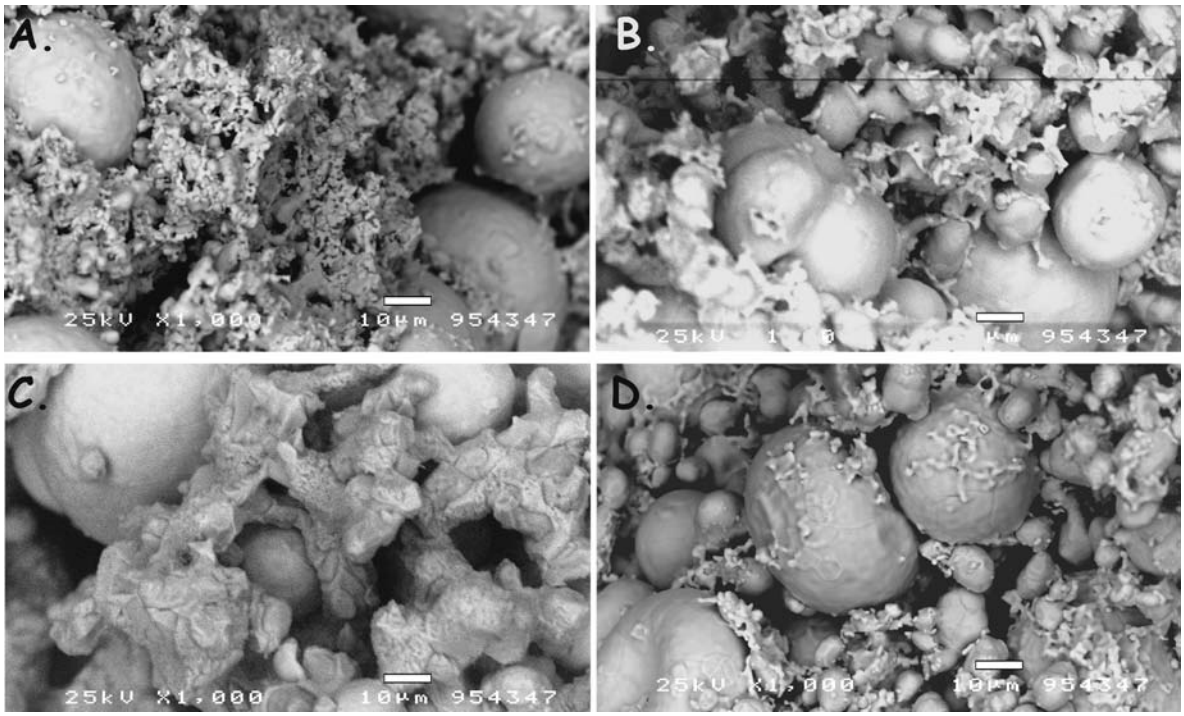

Figure 5 SEM micrographs showing fractured surfaces of the porous Ni/YSZ support after reduction at 1000°C. Samples sintered at 1500°C for 2 h prior to reduction. A: NYZ-7, B: NYZ-2, C: NYZ-3 and D: NYZ-1. Large spherical particles are YSZ; matrix is a mixture of Ni and fine YSZ.

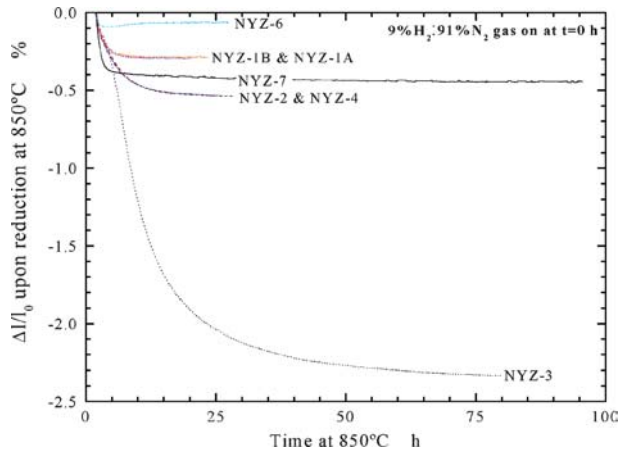

Figure 6 Linear dimensional change during reduction measured by dilatometry.

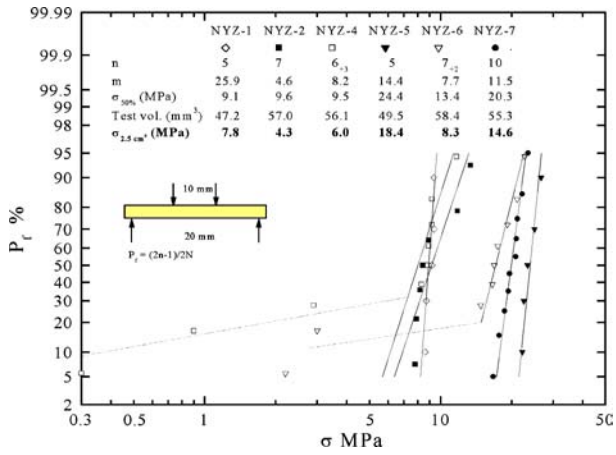

Figure 7 Weibull plot of the 4-point bending strength of as sintered anode supports.

powders (Table I). One type is based on black as-received NiO and large spherical coarse 8YSZ (calcined TZ-8Y TOSOH, $d_{50\%}$: 40 μm), while the other type is fabricated by calcined (1300°C/2 h) and ball milled black NiO ($d_{50\%}$: 5 μm) and MEL coarse SCY1291085 powder as the coarse 8YSZ ($d_{50\%}$ of 16 μm). The supports in the middle group are based on other combinations of the above precursor powders and different mixing schemes, which result in more porous and weaker supports.

Fig. 8 shows the fracture probability as a function of the bending force in a four-point bending test, for NYZ-7. The mean mechanical bending strengths before and after reduction (850°C) are not significantly different, both being around 20 MPa. While the Weibull modulus is somewhat lowered after reduction, the limited number of samples does not allow a firm conclusion to be drawn. The relatively small difference in strength between the as sintered and the reduced samples signifies that the strength is governed mainly by the three-dimensional network of YSZ.

3.4. Electrical conductivity

The four point electrical in-plane conductivity at 850°C of the eight support types fabricated reveals the same three groups.

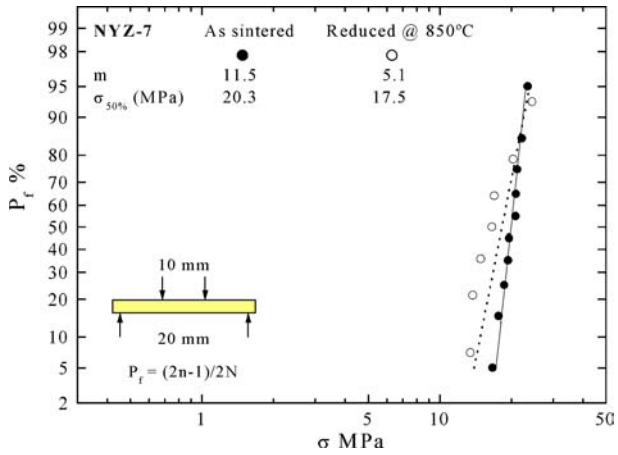

Figure 8 Bending strength of the strongest anode support type both as sintered and as reduced.

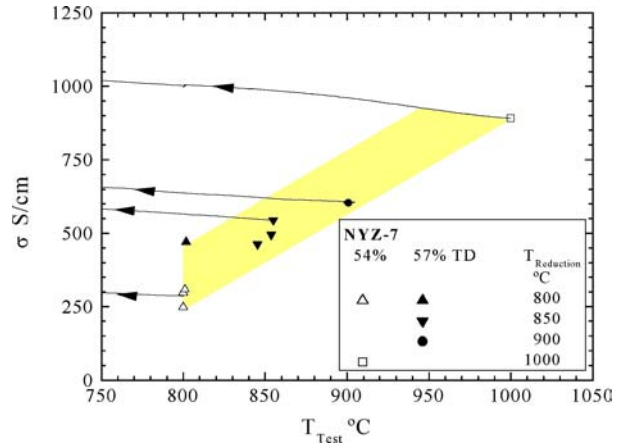

Figure 9 The symbols mark the in-plane electrical conductivity versus reduction and test temperature after 100 h of test where the samples were exposed to a current load of ≈7 A/cm^2. The lines with arrows show the change of conductivity upon cooling.

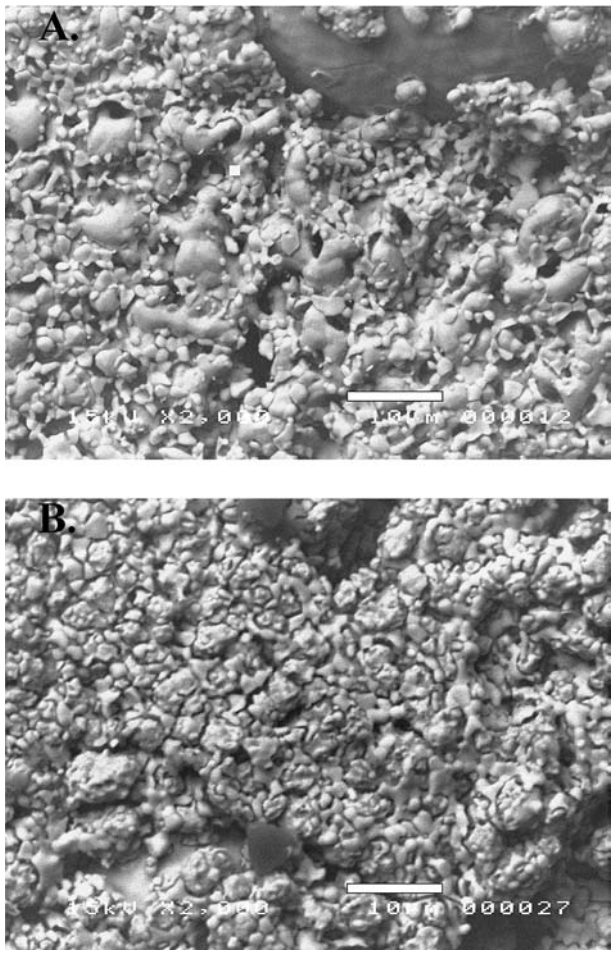

Figure 10 Microstructure of reduced NYZ-7. Scale-bar is 10 μm on both micrographs. Ni-particles are grey while YSZ is lighter. A: Reduced and tested for 100 h at 1000°C. B: Reduced and tested for 100 h at 800°C.

- The weakest support (NYZ-3) with no fine-grained zirconia shows a modest conductivity of 120 S/cm upon reduction and test at 850°C, and a limited degradation (5% within the first 100 h of test at 850°C).
- The intermediate group (NYZ-1, NYZ-2, NYZ-4, and NYZ-6) shows a variable conductivity upon reduction at 850°C ranging between 40 and 410 S/cm. However, all samples within this group show a rapid, undesirable degradation of 25–85% within the first 100 h of test at 850°C.
- The support types (NYZ-5 and NYZ-7) with the highest strength have a high conductivity of 550–600 S/cm upon reduction at 850°C, and a lower degradation of ≈10% within the first 100 h of test.

The last group of supports possesses the desired properties in the screening outlined above. The following detailed electrical conductivity is studied only on samples prepared from one of these supports (NYZ-7).

During the conductivity measurements, the final conductivity of the samples was found to be strongly dependent on the reduction temperature. This is illustrated in Fig. 9, where the electronic conductivity is plotted as function of the test temperature, which is identical to the reduction temperature. The samples reduced and tested at 1000°C show a factor 3 times higher conductivity than the similar samples reduced and tested at 800°C. The observed relation between reduction temperature and conductivity is almost linear. The microstructures of the two samples are shown in Fig. 10. Heating to a higher temperature did not improve the conductivity once the samples are reduced at a lower temperature as illustrated in Fig. 11. The sample reduced at 800°C (Fig. 10B) has a prominent YSZ network surrounding islands of Ni-particles, while the sample reduced at 1000°C has the same YSZ microstructure but with a continuous Ni phase (Fig. 10A). We speculate that the formation of a continuous Ni network at 1000°C is due to a redistribution of the freshly formed metal *while it is still surface active*. Accordingly, the failure to achieve the same effect at lower temperatures is explained by slow kinetics, while failure to achieve it upon subsequent high temperature treatment is explained by loss of surface activity of the nickel.

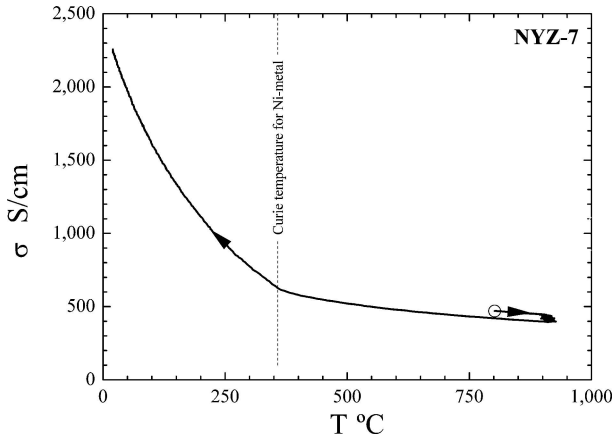

Figure 11 Conductivity of a sample reduced (57% TD) and tested at 800°C for 100 h followed by heating to 900°C at which temperature the sample was kept for another 100 h at a continuous current load of 7 A/cm^2 before cooling to room temperature.

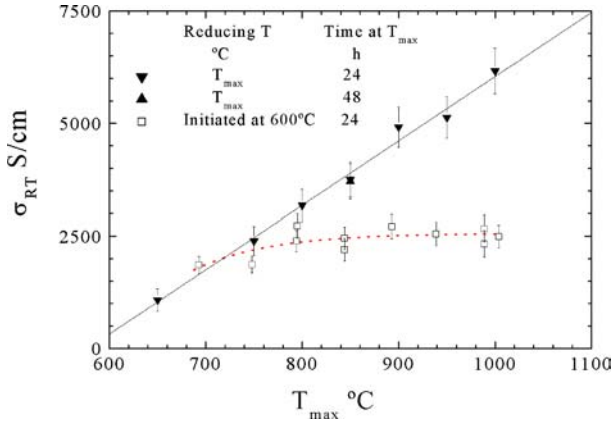

Figure 12 Conductivity at RT versus reduction temperature of NYZ-7 samples that not were exposed to current load before testing at RT. Closed symbols represent samples that were reduced and measured at the given temperature. Open symbols represent samples that were gradually heated under reducing conditions (reducing initiated at 600°C).

This explanation is consistent with conductivities presented in Fig. 12 for samples that were reduced in two different ways. Samples in the first group were reduced by heating to the maximum temperature in 9%H_2:91%N_2, while the samples in the other group were heated to the maximum temperature in air and then reduced by introducing 9%H_2:91%N_2. The first treatment was intended to simulate the conditions obtained upon the initial SOFC-stack heating. These samples show no influence of the maximum temperature on the conductivity. On the other hand, the second group show a linear relationship between conductivity and reduction temperature. These results are in good agreement with the results reported above (Fig. 9). The above results also indicate that aging under conditions of no current load is negligible for short aging times.

The effect of current load upon degradation is further emphasized by the results shown in Fig. 13, where the sample was twice exposed to a high continuous current

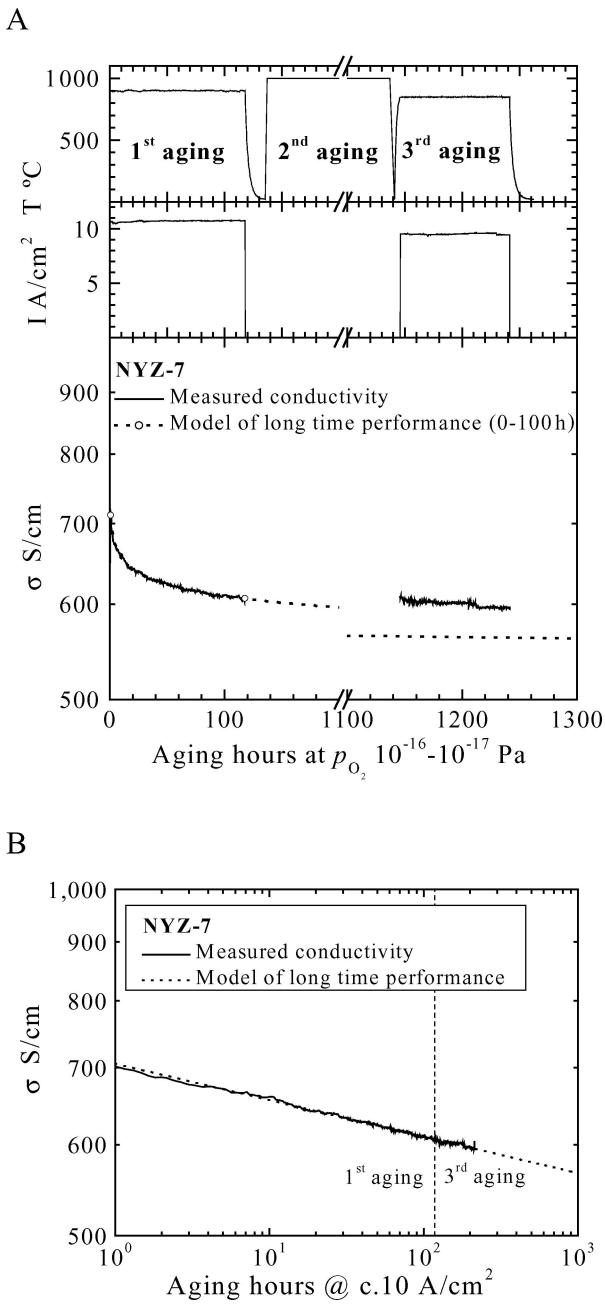

Figure 13 (A) Experimental log of an aging experiment. (B) Evolution of conductivity during the first and third aging where the sample was exposed to a current load of ≈10 A/cm^2.

load for 100 h, with a 1000 h aging without current load in between. The measured conductivity in the third aging cycle does not follow the development predicted from the first aging (Fig. 13A), taking the full aging time into consideration. However, the calculated model of long time performance fits perfectly when only the time where the sample was exposed to current load was considered Fig. 13B. The degradation of conductivity during load is illustrated in Fig. 14; upright and inverted triangles are reproduced results from Fig. 12, open circles represent the conductivity measured at room temperature after 100 h current load of 7 A/cm^2 at various temperatures. During

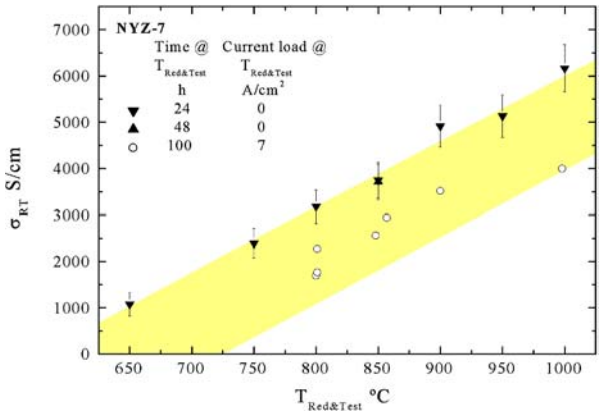

Figure 14 Conductivity measured at RT versus reduction temperature measured on samples with and without current load during the dwell time, open and closed symbols, respectively.

current load, redistribution of Ni is believed to take place and is thus the major reason for the measured degradation. The microstructure of the NiO network has a controlling influence on the Ni network formed upon reduction, and thus, on the electronic conductivity and its long-term stability. When no fine-grained 8YSZ powder is added, a much more coarse-grained NiO network is formed (NYZ-3, Fig. 4C). The fine-grained 8YSZ appear to be evenly distributed, where it acts as growth inhibitor for the Ni phase (Fig. 4A, B and D). This is even more pronounced in the reduced supports (Fig. 5).

3.5. Redox stability

One major disadvantage of using Ni-YSZ cermet based anodes in SOFC is the poor redox stability due to the large volume change upon oxidation/reduction that may cause an almost total disintegration. Fig. 15 shows preliminary results of redox cycling. In the figure, the conductivity is plotted as a function of time at 850°C for a sample that has undergone two redox cycles. The conductivity increases by a factor of two after the first cycle and remains at that level after the second cycle. However, the conductivity seems to degrade faster after redox cycling.

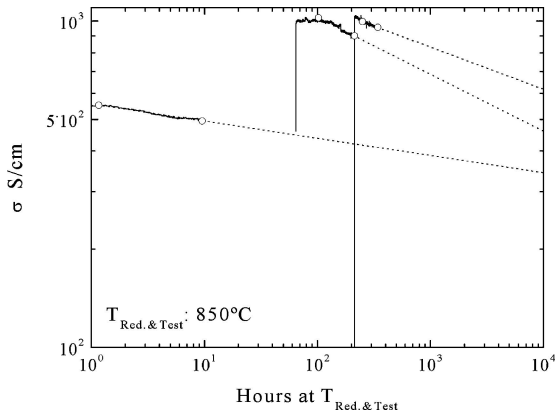

Figure 15 Redox-stability test of NYZ-7. The circles indicate the data end points for each of the three calculations of the longer time performance (dotted lines).

4. Summary and conclusion

Profiled anode supports have been successfully fabricated by water-based viscous processing. The mechanical strength and the conductivity have been examined as a function of composition and microstructure of the NiO/YSZ component. The mechanical strength of the optimised materials was not significantly altered upon reduction, indicating that the mechanical strength is determined mainly by the YSZ structure. The YSZ matrix holds the structure together such that redox stability, as measured by absence of degradation in the electronic conductivity, is achieved. In fact, the conductivity improved after redox cycling.

The overall conductivity and the stability of conductivity with time fulfil the requirements for use of these materials as anode supports or current collectors. Electronic conductivities of 250–900 S/cm have been achieved at 800 to 1000°C. The conductivity is significantly increased by raising the reduction temperature. However, once the material has been reduced, subsequent high temperature treatment in reducing conditions does not improve the conductivity. In other words, the samples show a memory of their thermal/redox history. It can be concluded that reduction should be carried out at the highest possible temperature in order to achieve the highest electronic conductivity.

Acknowledgment

Discussions with and the technical assistance of colleagues at RISØ and at IRD Fuel Cells A/S are appreciated. The present work was carried out under the EC project LOCO-SOFC, contract No. BRPR-CT97-0413.

References

1. N. CHRISTIANSEN, S. KRISTENSEN, H. HOLM-LARSEN, P. H. LARSEN, M. MOGENSEN, P. V. HENDRIKSEN and S. LINDEROTH, Status of SOFC Development at Haldor Topsøe/Risø, Luzern 2002.
2. P. H. LARSEN, C. BAGGER, S. LINDEROTH, M. MOGENSEN, S. PRIMDAHL, M. J. JØRGENSEN, P. V. HENDRIKSEN, B. KINDL, N. BONANOS, F. W. POULSEN and K. A. MAEGAARD, Status of the Danish SOFC Program,in "Solid Oxide Fuel Cells IV", edited by S. C. Singhal and M. Dokiya (The Electrochemical Society Proceedings Series, Pennington, NJ 1995) PV 95-1, p. 138.
3. K. A. NIELSEN, S. LINDEROTH, J. BILDE-SØRENSEN and P. H. LARSEN, in "Test and Performance Analysis of SOFC Stack Units", Luzern 2002.
4. M. MOGENSEN, S. SUNDE and S. PRIMDAHL, SOFC anode kinetics, in "Proceedings of the 17th Risø International Symposium on Materials Science: High Temperature Electrochemistry; Ceramics and Metals," edited by F. W. Poulsen et al. (Risø, Roskilde, Denmark, 1996).

5. N. Q. MINH, Development of thin-film solid oxide fuel cells for power generation applications, in "Solid Oxide Fuel Cells IV," edited by S. C. Singhal and M. Dokiya (The Electrochemical Society Proceedings Series, Pennington, NJ 1995) PV 95-1. p. 138.
6. J. P. ACKERMAN and J. E. YOUNG, Solid Oxide Fuel Cell having Monolithic Core. US Patent No. 4 476 198 (1984).
7. N. Q. MINH, C. R. HORNE, F. LIU, P. R. STASZAK, P. R. STILLWAGON and J. J. VAN ACKEREN, Forming and processing of monolithic solid oxide fuel cells, in edited by S. C. Singhal, Proc. First Intl. Symp. on Solid Oxide Fuel Cells. (Electrochemical Society, Inc. 1989) p. 307.
8. N. Q. MINH and R. A. GIBSON, Production of reduced-temperature solid oxide fuel cells by tape calendering, in"Proceedings First European Solid Oxide Fuel Cell Forum," edited by U. Bossel, (1995) p. 587.
9. N. Q. MINH, Ceramic fuel cells, *J. Am. Ceram. Soc.* **76**, (1993) 563.
10. K. KENDALL, E. WRIGHT and A. GOLDS, Co-formed components for solid oxide fuel cells, in "Solid oxide fuel cells (SOFC-IV)", edited by M. Dokiya, O. Yamamoto, H. Tagawa and S. C. Singhal, (Electrochemical Society, Inc. 1995) p. 229.
11. T. SHOHO and K. MORINAGA, in Fabrication of electrolyte for SOFC by extrusion, in "Solid oxide fuel cells (SOFC-IV)", edited by M. Dokiya, O. Yamamoto, H. Tagawa and S. C. Singhal (Electrochemical Society, Inc. 1995) p. 326.
12. H. ITOH, T. YAMAMOTO, M. MORI, T. HORITA, N. SAKAI, H. YOKOKAWA and M. DOKIYA, Configurational and electrical behaviour of Ni-YSZ cermet with novel microstructure for solid oxide fuel cell anodes. *J. Electrochem. Soc.* **144**(2) (1997) 641.
13. W. WEIBULL, A Statistical theory of the strength of materials. (Ingeniörsvetenskapsakademiens Handlingar nr. 151), (1931) 1.
14. J. D. SULLIVAN and P. H. LAUZON, Experimental probability estimators for weibull plots. *J. Mater. Sci. Letters* **5** (1986) 1245.
15. L. GRAHL-MADSEN, Oxid baseret konstruktionskeramik: Fremstilling og karakterisering. unpubl. Ph.D. thesis DTU, Denmark, (1988) p. 1.

Received 9 April 2004
and accepted 25 May 2005